A Wigner function approach to near-field acoustic holography - theory and experiments

Tanner, Gregor[1]
University of Nottingham
University Park, Nottingham NG7 2RD, UK

Madenoor Ramapriya, Deepthee, Gradoni, Gabriele and Creagh, Stephen C
University of Nottingham
University Park, Nottingham NG7 2RD, UK

Moers, Elise and Lopéz Arteaga, Inés
Technische Universiteit Eindhoven
PO Box 51, 35600 MB Eindhoven, NL

ABSTRACT

We discuss the concept of Wigner transformation in the context of propagating stochastic acoustic signals in the near- and farfield. The starting point is a statistical description of the sound field in terms of spatial correlation functions. A phase space approach based on Wigner functions is then adopted and the corresponding free field propagator is introduced. Acoustic data are acquired in an experiment using an 'acoustical camera'; the sound pressure emanating from a vibrating rectangular plate is measured on a 32×32 microphone array in coincidence. Measurements and simulations are compared at different heights above the source plane. It is demonstrated that the Wigner function approach provides a stable tool to propagate correlation data.

1. INTRODUCTION

Modelling the propagation of sound from vibrating structures is of fundamental importance in the context of sound radiation, Nearfield Acoustical Holography (NAH) [1], and noise and vibration control [2]. To optimise the external sound field, it is important to determine the wave amplitude distribution at source level as represented,

---

[1] gregor.tanner@nottingham.ac.uk

for example, by the sound pressure level in a fluid near the surface of a vibrating built-up structure [3]. The structure-borne sound distribution in the solid can then be deduced from the pressure field in the fluid (or vice versa) by using the relations between the (near-field) pressure and the vibrational modes of the structure [4]. Radiation from both regular structures, such as rectangular plates and cylindrical or spherical bodies (see [5] for an overview) and from arbitrarily shaped surfaces, see e.g. [6–9], have been considered in detail. Sound pressure measurements in the very near-field, measured either by intensity probes or by microphones and microphone arrays, have been described in [10–12].

In this paper, we discuss the so-called *Wigner function* (WF) approach in the context of noise radiation and NAH. We will in particular demonstrate that the WF approach mitigates some of the problems in NAH [13] - such as blow-up of the back-propagated field due to noise-induced evanescent contributions - in an elegant way. The WF approach has its origin in quantum mechanics [14] and has more recently found widespread attention in optics [15–17] and radio frequency (RF) radiation [18, 19]. The WF formalism offers a direct route to pure ray-tracing approximations in an operator implementation [18, 20], while still capturing in its exact formulation the full wave dynamics. It is particularly powerful in the case of incoherent or noisy sources, allowing a prediction of the radiated intensity even in the absence of full phase characterisation of the source. The method exploits a connection between the spatial field-field *correlation function* (CF) and the WF [21–23]. In [18], efficient propagation of CFs using ray propagation in phase-space is demonstrated, an extension of the formalism to radiation in confined space such as cavities is described in [20].

The routine use of microphone arrays in acoustic experiments, measuring sound pressure at thousands of positions in parallel [12, 13], provides the ideal background for spatial correlation measurements in the time domain - an important input and thus a prerequisite for the WF approach. In particular, we propose here to propagate a statistical quantity - the CF for noisy signals after suitable time averaging - directly and we will demonstrate how this can be done efficiently using the WF approach. Noise contributions are naturally suppressed here through time averaging and evanescent components can be naturally filtered out avoiding blow-up problems in the back-propagation. We note in passing that *n*-point measurements are challenging in the context of electromagnetic radiation in the RF range for $n > 2$ [19, 24, 25], whereas the same is not true for acoustics where microphone arrays can easily measure time-dependent acoustic fields for up to 1000 positions simultaneously.

The paper is structured as follows: In Sec. 2.1, we describe the experimental set-up for measuring radiation off a rectangular plate with a 32×32 microphone array. In Sec. 3, we present the basic theory of the WF approach considering radiation into free space from an extended planar source. The experimental measurements are analysed with WF methods in Sec. 4 and theoretical simulations are compared with experiments. In particular, the potential of WF techniques for nearfield holography will be demonstrated. We show that WF techniques are ideally suited (i) to filter out blow-up in the reconstructed source, and (ii) to obtain source distributions without a priori knowledge of the plate geometry.

2. PROPAGATION OF SOUND FROM EXTENDED, STOCHASTIC SOURCES

Sound radiation from complex structures is often stochastic in nature due to the complexity of the underlying stucture-borne sound field and broadband excitation
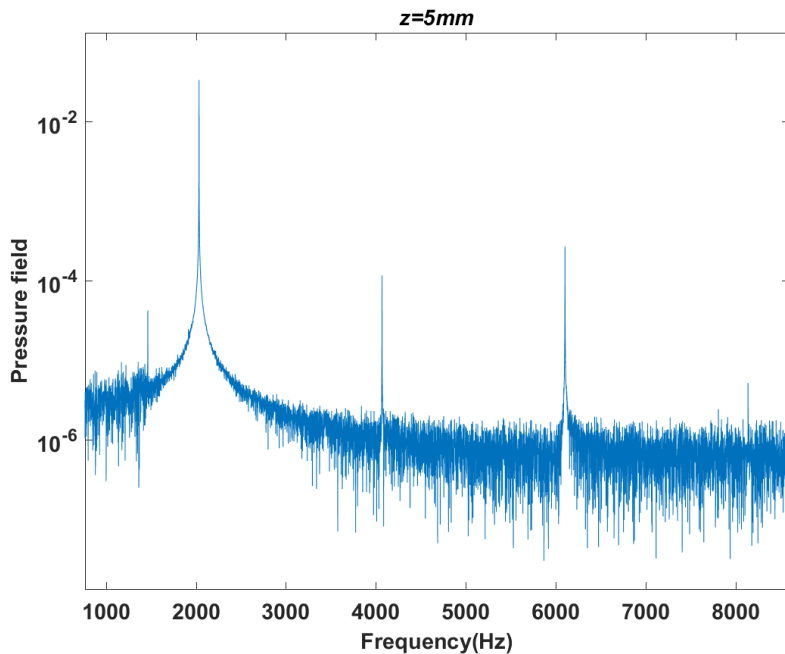
Figure 1: Power spectrum of the measured sound pressure at (x, y) = (0mm, 0mm), as a function of frequency, with driving frequency f = 2034 Hz taken at a distances z = 5 mm above the plate.

through incoherent force-loading conditions. A statistical description of the sound field is then appropriate. The key objectives of this paper are to describe the propagation of such statistical data - particularly the spatial correlation function (CF) - and to provide interpretation of its spatial and directional distribution through the Wigner function (WF).

The feasibility of the approach is established by applying it to the measured data obtained from the experimental set-up described in Sec. 2.1 and also in [12, 13].

2.2.1. Experimental set-up

A prerequisite for the analysis performed in this paper is the ability to measure sound pressure field distributions simultaneously in time at different positions in space above a source plane. While this still poses a considerable challenge in the radio frequency range for radiation in an electromagnetic context (as outlined in [18, 19, 25]), in the acoustic domain there are commercially available microphone arrays [26] which make it possible to measure the sound amplitude at thousands of positions simultaneously. Below we report the experimental setup for carrying out a sound recording measurement above a vibrating simply-supported rectangular aluminium plate. We emphasise that the measurements and analysis performed are appropriate to completely characterise stochastic sources and do not rely on any pre-existing analysis of the source plate in terms of eigenfunction expansions as suggested in [12, 13].

The experimental set-up is described in [12, 13]. Simply-supported boundary conditions are obtained approximately by loosely clamping the plate in an aluminium frame. The frame is at its inner sides equipped with thin cylindrical wires such that rotation at the edges is possible. The width and length of the plate are L_x = 203mm and L_y = 303mm, respectively. The thickness is h = 5mm. The plate is excited at the bottom by a shaker of type BK-LDS V201 [27].

A *Sorama CAM1K* microphone array with 1024 microphones is positioned above the plate [26]. The microphones are fixed on a 32×32 grid frame with equidistant positions having an inner spacing of 20mm. The sample frequency of the microphone array is 46.875 kHz. The data are gathered for 1s and saved for further processing with Matlab©. All measurements are performed in a semi-anechoic room. The distance
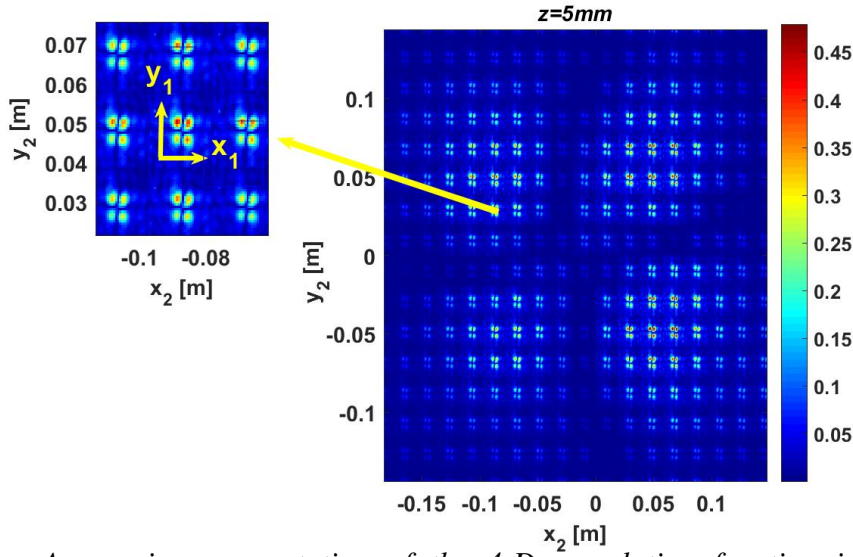
Figure 2: A mosaic representation of the 4-D correlation function in frequency representation. The pressure fields are measured at a distance of $z = 5mm$.(Online version in colour.)

between the microphones and the plate can be varied at discrete steps with heights $z_h = $ 5mm, 30mm and 50mm, measured from the top surface of the plate to the lower surface of the microphones. The microphones are box-shaped of dimensions 4mm $\times$ 3mm $\times$ 2mm and soldered to the grid points of the Sorama array.

A typical power spectrum of the pressure field at a fixed point, here in the middle of the plate at $(x, y) = $ (0mm,0mm), is shown in Fig. 1. The main features are peak responses at multiple integer harmonics of the driving frequency $f = $ 2034 Hz, that is, at $f = $ 2034 Hz, 4068 Hz, 6102 Hz and 8136 Hz and are a consequence of the narrowband, periodic driving mechanism. We would like to emphasise that the measurement and propagation procedures described in this work apply also to more complex forcing mechanisms, see [25]. Correlation measurements reported in the remainder of the paper are restricted to these peak frequencies.

2.2.2. Characterisations of radiated fields using correlation functions

We will in the following consider sound radiation off a planar rectangular plate. The sound pressure level is denoted $\phi(\mathbf{r}, z; t)$ where $\mathbf{r} = (x, y)$ denote the coordinates in the plane of the source and z measures the distance normal to the source. We choose $-L_x/2 \leq x \leq L_x/2$ and likewise $-L_y/2 \leq x \leq L_y/2$, where L_x, L_y are the dimensions of the plate..

The time-spatial correlation function is defined as

$$C_z(\mathbf{r}_1, \mathbf{r}_2; \tau) = \lim_{T \to \infty} \frac{1}{T} \int_0^T \phi(\mathbf{r}_1, z; t + \tau) \phi(\mathbf{r}_2, z; t) \, \mathrm{d}t. \tag{1}$$

In the frequency domain, this field-field CF is represented by the Fourier transform

$$\Gamma_z(\mathbf{r}_1, \mathbf{r}_2; \omega) = \int_{-\infty}^{\infty} \mathrm{e}^{-\mathrm{i}\omega\tau} C_z(\mathbf{r}_1, \mathbf{r}_2; \tau) \, \mathrm{d}\tau. \tag{2}$$

To visualise the four-dimensional CF $\Gamma(\mathbf{r}_1, \mathbf{r}_2, \omega)$ obtained from the measurement date over the full range of accessible $(\mathbf{r}_1, \mathbf{r}_2)$ values, we have chosen a mosaic representation as displayed in Fig. 2, here at the excitation frequency 2034 Hz. We choose a grid of coordinate points in the x_2, y_2 plane and then obtain the CF in terms of the variables x_1, y_1 for fixed x_2, y_2, see the LHS of Fig. 2. The driving frequency is close to the $(2, 2)$ flexural eigenmode of the plate, which has been measured to be at 1872 Hz [13] and which also dominates the correlation pattern.

In the following we will consider $\Gamma(\mathbf{r}_1, \mathbf{r}_2, \omega)$, measured and predicted for frequency values $f_0 = 2034$ Hz and 4068 Hz at different heights above the source plane. For the propagated correlation functions, the pressure fields measured at $z = 5$mm serve as the input data for the correlation-function propagator described in the following section. Note that for a rectangular plate ideal simply supported boundary conditions provide a particularly simple description of the eigenmodes of the flexural dynamics in the form

$$w_{n,m}(x, y) = A_{nm} \sin\left[n\pi\left(\frac{x}{L_x} + \frac{1}{2}\right)\right] \sin\left[m\pi\left(\frac{y}{L_y} + \frac{1}{2}\right)\right],$$

with (n, m) being positive integers.

3. PROPAGATION OF CORRELATION DATA IN PHASE SPACE

The propagation into free space of measured spatial correlations can be predicted numerically by Fourier transforming to a representation of the data in terms of momentum (or direction) variables. We emphasise in our analysis the Wigner function, which not only allows efficient propagation of the data, but also provides a simple interpretation of this propagation in terms of transport along rays in phase space.

3.3.1. Propagation in momentum and in phase space

We begin by transforming the CF to a momentum representation defined by

$$\tilde{\Gamma}_z(\mathbf{p}_1, \mathbf{p}_2, \omega) = \iint e^{-ik\mathbf{p}_1 \cdot \mathbf{r}_1} \Gamma_z(\mathbf{r}_1, \mathbf{r}_2; \omega) e^{ik\mathbf{p}_2 \cdot \mathbf{r}_2} d\mathbf{r}_1 d\mathbf{r}_2, \tag{3}$$

where $k\,\mathbf{p}$ is the wave vector component in the (x, y)–plane and k denotes the free-space wavenumber. The propagation of $\tilde{\Gamma}_z$ in z direction can then be described as [18]

$$\tilde{\Gamma}_z(\mathbf{p}_1, \mathbf{p}_2) = e^{ik(z-z_0)[T(\mathbf{p}_1) - T^*(\mathbf{p}_2)]} \tilde{\Gamma}_{z=z_0}(\mathbf{p}_1, \mathbf{p}_2), \tag{4}$$

where z_0 denotes the source plane distance, here $z_0 = 5mm$. We leave out the explicit ω dependence for convenience. Furthermore, the normal component of the unit wave vector is defined as ([28], page 342)

$$T(\mathbf{p}) = \begin{cases} \sqrt{1 - p^2} & \text{for } p^2 \leq 1 \\ i\sqrt{p^2 - 1} & \text{for } p^2 > 1. \end{cases} \tag{5}$$

This applies both to evanescent ($p^2 > 1$) and propagating ($p^2 \leq 1$) regimes. Joint positional and directional information can be extracted from the CF through the WF obtained from (4) by making the coordinate rotation

$$\begin{aligned} \mathbf{p} &= (\mathbf{p}_1 + \mathbf{p}_2)/2, \\ \mathbf{q} &= \mathbf{p}_1 - \mathbf{p}_2 \end{aligned} \tag{6}$$

and then taking an inverse Fourier transform in the displacement variable $\mathbf{q}$

$$W_z(\mathbf{r}, \mathbf{p}) = \left(\frac{k}{2\pi}\right)^d \int e^{ik\mathbf{r} \cdot \mathbf{q}} \tilde{\Gamma}_z(\mathbf{p}, \mathbf{q}) \, d\mathbf{q}, \tag{7}$$

where $\mathbf{r} = (\mathbf{r}_1 + \mathbf{r}_2)/2$, and d is the dimension of the transverse direction. We will focus in what follows on full 3D simulations with $\mathbf{r} = (x, y)$ and thus $d = 2$.

Both the CF and WF representations of propagating and evanescent wave densities have been studied extensively for a planar source in the context of electromagnetic waves [18, 19, 25]. An explicit propagator for the WF can be obtained by taking the Wigner transform, Eq. (7), of both the propagated and the source CF in (4) and writing formally [18, 25]

$$W_z(\mathbf{r}, \mathbf{p}) = W_{z=z_0}(\mathbf{r}, \mathbf{p}) *_{\mathbf{r}} \mathcal{G}_z(\mathbf{r}, \mathbf{p}),\tag{8}$$

where $*_{\mathbf{r}}$ indicates a convolution with respect to the variable $\mathbf{r}$ only and the WF propagator in free space takes the form

$$\mathcal{G}_z(\mathbf{r}, \mathbf{p}) = \left(\frac{k}{2\pi}\right)^d \int e^{-k(z-z_0)(T(\mathbf{p}+\mathbf{q}/2)-T^*(\mathbf{p}-\mathbf{q}/2))} e^{ik\mathbf{q}\cdot\mathbf{r}} \, d\mathbf{q}.\tag{9}$$

The propagated correlation function can be retrieved by performing an inverse Fourier transform of the WF with respect to $\mathbf{p}$, which is defined as

$$\Gamma_z(\mathbf{r}, \mathbf{s}) = \left(\frac{k}{2\pi}\right)^d \int e^{ik\mathbf{p}\cdot\mathbf{s}} \, W_z(\mathbf{r}, \mathbf{p}) d\mathbf{p},\tag{10}$$

in which we use the rotated coordinates

$$\begin{aligned}\mathbf{r} &= (\mathbf{r}_1 + \mathbf{r}_2)/2,\\ \mathbf{s} &= \mathbf{r}_1 - \mathbf{r}_2\end{aligned}\tag{11}$$

to label position pairs and we note that $\mathbf{r}$ and $\mathbf{s}$ are respectively conjugate to the rotated momentum variables $\mathbf{q}$ and $\mathbf{p}$ in (6).

Equation (8) is an ideal starting point for short wavelength and deep near-field approximations. The ray-tracing limit, along with higher-order corrections, emerges naturally in the large k limit for propagating components, for which $p^2 < 1$ [18]; one obtains in leading order

$$W_z(\mathbf{r}, \mathbf{p}) \approx W_{z=z_0}\left(\mathbf{r} - \frac{(z-z_0)\,\mathbf{p}}{T(\mathbf{p})}, \mathbf{p}\right), \quad |p|^2 < 1.\tag{12}$$

Evanescent decay and an associated diffusion process dominate the small z/λ and $p \gg 1$ limit where $\lambda = 2\pi/k$ is the wavelength [25]. We will not dwell on these approximate approaches in what follows and will in general use the full propagator (8) providing numerically exact results in the analysis section, Sec. 4.

4. RESULTS AND ANALYSIS OF THE MEASURED DATA

4.4.1. Correlation functions

The acoustic data are obtained by exciting a rectangular plate at the right upper quarter of the plate with a shaker. The experiment was repeated at different heights thus measuring sound as it is transported away from the plate. We will in the following focus on results obtained for an excitation frequency of 2034 Hz. Following on from the theoretical considerations in Sec. 3, we first construct the spatio-temporal correlation function from the acoustic pressure data $\phi(\mathbf{r}, t)$ measured at the microphone position $\mathbf{r} = (x, y)$. The correlation function, Eq. (1), is obtained approximately from measurements taken over a finite time interval T, that is,

$$C(\mathbf{r}_1, \mathbf{r}_2, \tau) = \langle \phi(\mathbf{r}_1, t)\phi^*(\mathbf{r}_2, t - \tau)\rangle = \frac{1}{T}\int_0^T \phi(\mathbf{r}_1, t)\phi^*(\mathbf{r}_2, t - \tau)\,dt.\tag{13}$$
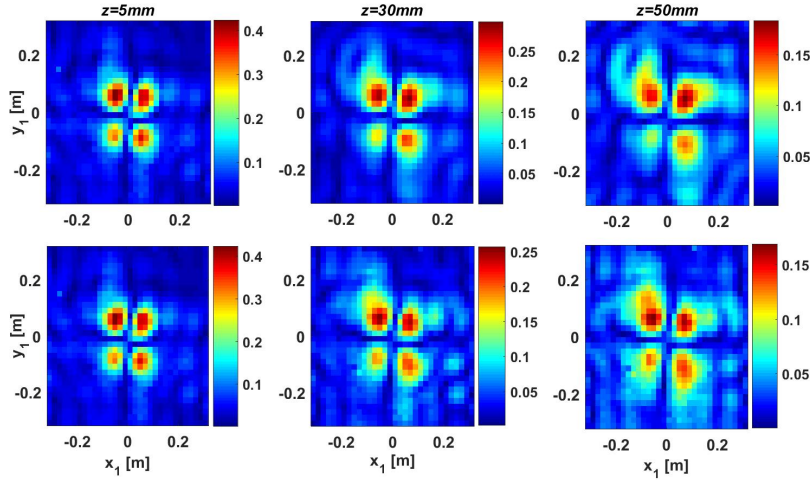
Figure 3: CF at frequency $f = 2034$ Hz; results obtained from numerical computations (1st row) are compared with the experimental data (2nd row) at different heights above the plate with $x_2 = 9$mm, $y_2 = 5$mm, fixed.

For convenience, we use continuous variables (x, y, t) throughout, although it is understood that both the spatial positions and the time are discretised in the measurements themselves. On moving from the time domain to the frequency domain, we perform a Fourier transform with respect to the time displacement τ in order to obtain the spatial correlation function $\Gamma(\mathbf{r}_1, \mathbf{r}_2, \omega)$ as spelled out in Eq. (2). The intensity is obtained as

$$I(\mathbf{r}, \omega) = \Gamma(\mathbf{r}, \mathbf{r}, \omega) = \left\langle |\hat{\phi}(\mathbf{r}, \omega)|^2 \right\rangle. \tag{14}$$

The CF in Fig. 3 is shown here as function of x_1, y_1 at fixed $x_2 = 9$mm, $y_2 = 5$mm for $f_0 = 2034$ Hz. We observe four prominent peaks in the CF indicating a strong contribution from the $(2, 2)$ eigenmmode of plate vibration. When moving from the measurement plane at $z_0 = 5$mm closest to the plate to $z = 30$mm and $z = 50$mm, one observes a broadening of the peaks with increasing distance from the plate: this is predicted using the phase space propagation method described in the previous section. The numerical (upper row) and the experimental data (lower row) are in good agreement. Similar results are found for the other dominant frequencies at 4068 Hz, 6102 Hz and 8136 Hz.

The intensity defined in (14) is shown in Fig. 4 for the frequency $f = 4068$Hz. The top two rows display the intensity in the (x, y) - plane and show features similar to the correlation data in Fig. 3. The bottom row in Fig. 4 displays the intensity along the line $y = 130$mm. A comparison is made here between the measured CF (black line), the numerically exact CF propagator, Eqn. (8) (green line) and the ray tracing (or linear) approximation, Eqn. (12) (red line). One observes that the measured and exactly propagated data agree well throughout. The linear approximation captures the overall behaviour well, but does not agree when it comes to details such as the peak heights. This behaviour can be observed for other cuts along fixed y both in regions with high and low overall intensity.

4.4.2. Propagated Wigner functions

It is also instructive to consider the WF itself, in particular as it is possible to extract dynamical information from this representation and thus to reach a better understanding of the propagation mechanism.
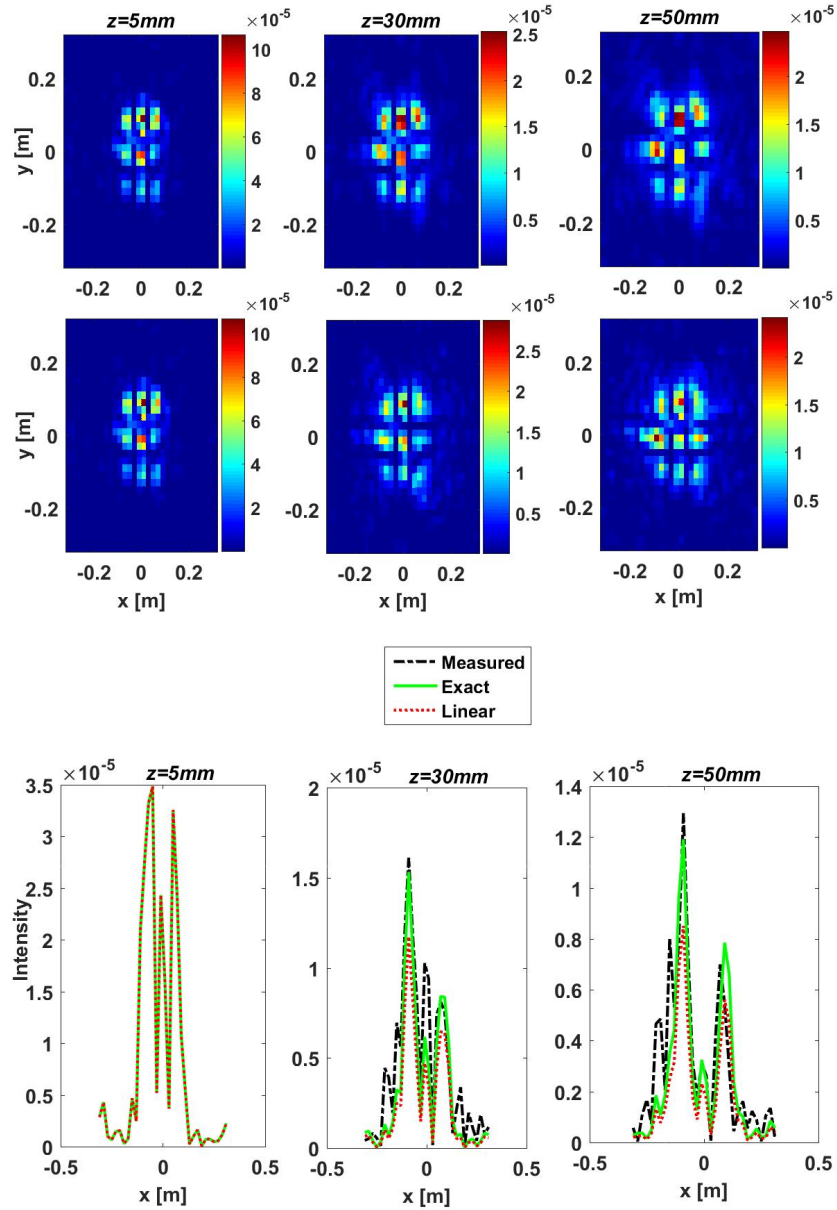
Figure 4: Intensity at different distances above the plate at f = 4068 Hz. Top rows: Intensity in the full x, y plane; bottom row: intensity along the line y = 130mm comparing measured data (black/ dashed line) with numerically exact propagated data (green/ solid line) and those obtained using the linear approximation (red/dotted line).
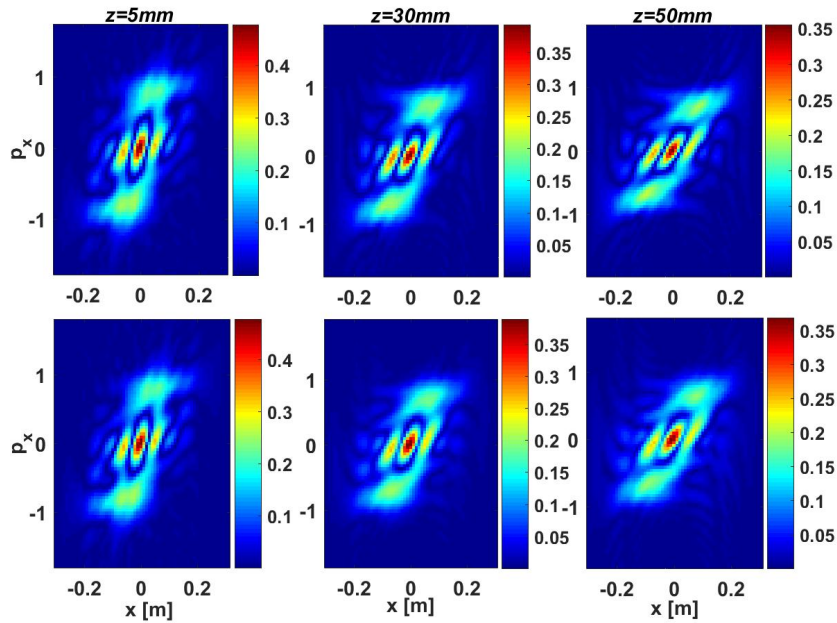
Figure 5: WF of the pressure fields in (x, p_x) space for fixed $(y, p_y) = (0, 0)$ measured (top row) and the WF obtained using the propagator (bottom row) for various heights above the plate and at $f = 2034$ Hz.

In Fig. 5, the WF $W_z(\mathbf{r}, \mathbf{p})$ is plotted, here as a function of (x, p_x) while keeping $y = 0$, $p_y = 0$ fixed. Again, a comparison between the propagated and measured WFs is shown at $f = 2034$ Hz. The agreement is very good - not surprisingly after what has been reported in the previous section. We also observe a 'shearing' of the WF where the slope or shearing angle increases with distance from the source. The shearing can be interpreted in terms of a ray-dynamics: waves or rays with $p_x = 0$ leave in a direction normal to the plate, rays with $p_x \approx \pm 1$ emanate tangentially to the plate. When moving the detection plane away from the source, rays with larger absolute values of p_x will travel further in the x direction, see Eq. (12). When projected onto the spatial representation, this shearing leads to the observed widening of the correlation peaks in Fig. 3.

Note that due to the wavenumber scaling chosen in, for example, Eqn. (7), p_x and p_y larger than 1 in absolute values can be identified with evanescent waves leading to exponential decay in z direction. From the WF shown in Fig. 5, we conclude that evanescent waves are not present even in the near field and that propagating contributions related to the range $-1 < p_x < 1$ dominate; (note that the wavelength in air is roughly 15 cm at 2 kHz, so all measurements are done in the near-field). This indicates, that the shaker does not significantly excite evanescent components at the frequencies considered.

5. CONCLUSIONS

We have demonstrated the feasibility of using Wigner functions to predict and interpret the evolution of statistically characterised acoustic fields as one moves away from the source. In particular, the measurements of the pressure fields near the source by the microphone array has been demonstrated to provide enough spatial resolution to serve as input for a detailed numerical predictions of intensities and spatial correlation functions away from the source. Although the particular driving mechanism used in the experiment can be understood using coherent models of the field amplitudes themselves [12], we emphasise that the theoretical approach outlined in this paper applies equally to scenarios

where the source is completely stochastic and characterised only through statistical properties such as (time-averaged) correlation functions.

6. ACKNOWLEDGMENTS

7. REFERENCES

[1] E. G. Williams and J. D. Maynard. Holographic imaging without the wavelength resolution limit. *Phys. Rev. Lett.* , 45:554 – 557, 1980.

[2] C. Hansen and S. Snyder. *Active control of noise and vibration.* CRC press, 2nd edition, 2012.

[3] H.-K. Lee and Y.-S. Park. A near-field approach to active control of sound radiation from a fluid-loaded rectangular plate. *J. Sound. Vib.*, 196:579 – 593, 1996.

[4] L. Cremer, M. Heckl, and B.A.T. Petersson. *Structure-Borne Sound: Structural Vibrations and Sound Radiation at Audio Frequencies.* Springer-Verlag, Berlin, Heidelberg, 2005.

[5] E. G. Williams. *Fourier Acoustics: Sound Radiation and Nearfield Acoustical Holography.* Academic Press, 1999.

[6] W. A. Veronesi and J. D. Maynard. Digital holographic reconstruction of sources with arbitrarily shaped surfaces. *J. Acoust. Soc. Am.*, 85:588 – 598, 1989.

[7] S. F. Wu and X. Zhao. Combined Helmholtz equation-least squares method for reconstructing acoustic radiation from arbitrary shaped objects. *J. Acoust. Soc. Am.*, 112:179 – 188, 2002.

[8] N. Valdivia and E. G. Williams. Implicit methods of solution to integral formulations in boundary element based nearfield acoustic holography. *J. Acoust. Soc. Am.*, 126:149 – 157, 2009.

[9] D. J. Chappell and P. J. Harris. A Burton - Miller inverse boundary element method for near-field acoustic holography. *J. Acoust. Soc. Am.*, 116:1559 – 1572, 2004.

[10] C. Pezerat, Q. Leclaire, N. Totaro, and M. Pachebat. Identification of vibration excitations from acoustic measurements using near field acoustic holography and the force analysis technique. *J. Sound. Vib.*, 326:540 – 556, 2009.

[11] J. Prezelj, P. Lipar, A. Belsak, and M. Cudina. On acoustic very near field measurements. *Mechanical Systems and Signal Processing*, 40:195 – 207, 2013.

[12] E. Moers, I. Lopez-Arteaga, and H. Nijmeijer. Plate Modal Amplitude Determination from Microphone Array Data. In *The 22nd International Congress on Sound and Vibration (*ICSV22*)*, volume 1, pages 57 – 64, 2015.

[13] E. Moers. *Towards real-time detection of plate vibrations from acoustic measurements*. PhD-thesis. Eindhoven University of Technology Library, 2016.

[14] M. Hillery, R.F. O'Connell, M.O. Scully, and E.P. Wigner. Distribution functions in physics: Fundamentals. *Physics Reports*, 106(3):121 – 167, 1984.

[15] M. J. Bastiaans. The wigner distribution function and hamilton's characteristics of a geometric-optical system. *Optics Communications*, 30(3):321 – 326, 1979.

[16] A. Torre. *Linear Ray and Wave Optics in Phase Space: Bridging Ray and Wave Optics via the Wigner Phase-Space Picture*. Elsevier Science, 2005.

[17] Miguel A. Alonso. Wigner functions in optics: describing beams as ray bundles and pulses as particle ensembles. *Adv. Opt. Photon.*, 3(4):272–365, Dec 2011.

[18] G. Gradoni, S. C. Creagh, G. Tanner, C. Smartt, and D. W. P. Thomas. A phase-space approach for propagating field-field correlation functions. *New Journal of Physics*, 17(9):093027, 2015.

[19] G. Gradoni, L. R. Arnaut, S. C. Creagh, G. Tanner, M. H. Baharuddin, C. Smartt, and D. W. P. Thomas. Wigner-function-based propagation of stochastic field emissions from planar electromagnetic sources. *IEEE Transactions on Electromagnetic Compatibility*, 60(3):580–588, June 2017.

[20] S. C. Creagh, G. Gradoni, T. Hartmann, and G. Tanner. Propagating wave correlations in complex systems. *Journal of Physics A: Mathematical and Theoretical*, 50(4):045101, 2017.

[21] R. G. Littlejohn and R. Winston. Corrections to classical radiometry. *J. Opt. Soc. Am. A*, 10(9):2024–2037, Sep 1993.

[22] R. Winston, A. D. Kim, and K. Mitchell. Measuring radiance: a paradigm for coherence optics in six-dimensional phase space. *Journal of Modern Optics*, 53(16-17):2419–2429, 2006.

[23] T. Dittrich and L. A. Pachón. Time-Domain Scars: Resolving the Spectral Form Factor in Phase Space. *Phys. Rev. Lett.*, 102:150401, Apr 2009.

[24] J. A. Russer and P. Russer. Modeling of noisy em field propagation using correlation information. *IEEE Transactions on Microwave Theory and Techniques*, 63(1):76–89, Jan 2015.

[25] G. Gradoni, D. M. Ramapriya, S. C. Creagh, G. Tanner, M. H. Baharuddin, H. Nasser, C. Smartt, and D. W. P. Thomas. Near-field scanning and propagation of correlated low-frequency radiated emissions. *IEEE Transactions on Electromagnetic Compatibility*, PP(99):1–9, 2017.

[26] Sorama. Sorama CAM1K, www.sorama.eu/CAM1K, 2017.

[27] Brüel & Kjær. Permanent magnet shaker LDS V201, 2017 www.bksv.com/en/products/shakers-and-exciters.

[28] G. Barton. *Elements of Green's Functions and Propagation: Potentials, Diffusion, and Waves*. Oxford science publications. Clarendon Press, 1989.